Acknowledgment. We are grateful to the National Science Foundation for financial support of this research, the Office of Academic Computing at UCLA for use of the computer facilities, and Professor Matthew Platz of The Ohio State University for helpful discussions.

Registry No. $H_3C\ddot{C}H$, 4218-50-2; $H_3C\ddot{C}Cl$, 31304-51-5; $H_3C\ddot{C}OH$, 30967-49-8; $H_3C\ddot{C}OMe$, 65092-80-0; $H_3C\ddot{C}CH{=}CH_2$, 98115-38-9; $H\ddot{C}CH_2CH{=}CH_2$, 90566-94-2.

Reaction Path Following in Mass-Weighted Internal Coordinates

Carlos Gonzalez and H. Bernhard Schlegel*,†

Department of Chemistry, Wayne State University, Detroit, Michigan 48202 *(Received: November 1, 1989; In Final Form: April 3, 1990)*

Our previous algorithm for following reaction paths downhill (*J. Chem. Phys.* **1989**, *90*, 2154), has been extended to use mass-weighted internal coordinates. Points on the reaction path are found by constrained optimizations involving the internal degrees of freedom of the molecule. The points are optimized so that the segment of the reaction path between any two adjacent points is described by an arc of a circle in mass-weighted internal coordinates, and so that the gradients (in mass-weighted internals) at the end points of the arc are tangent to the path. The algorithm has the correct tangent vector and curvature vectors in the limit of small step size but requires only the transition vector and the energy gradients; the resulting path is continuous, differentiable, and piecewise quadratic. Reactions paths for $CH_4 + H \rightarrow CH_3 + H_2$, $HCN \rightarrow CNH$, $F^- + CH_3F \rightarrow FCH_3 + F^-$, and $C_2H_5F \rightarrow C_2H_4 + HF$ are calculated and the results are compared to the paths obtained with mass-weighted Cartesians and with internal coordinates without mass-weighting.

1. Introduction

The concept of the reaction pathway has become important in the study of potential energy surfaces for chemical reactions. In general, the reaction path can be defined as the curve on the potential energy surface connecting the reactants and products through the transition state. This curve can be found by following the steepest descent path or minimum energy path (MEP) from the transition state toward reactants and products. When mass-weighted Cartesian coordinates are used, the path becomes the intrinsic reaction coordinate (IRC) discussed by Fukui.[1]

In a previous paper, a new reaction path algorithm was presented that is capable of following curved reaction paths with reasonable large step sizes.[2] The efficiency and stability of the method was demonstrated on a model surface and various simple reactions by using internal coordinates without mass-weighting. To study reaction dynamics, it is desirable to include mass-weighting in the determination of the reaction path.

In the present work, our previous algorithm[2] is modified to include the effects of the atomic masses. The new algorithm for following the intrinsic reaction coordinate in mass-weighted internal coordinates is tested on the following reactions: $CH_4 + H \rightarrow CH_3 + H_2$, $HCN \rightarrow HNC$, $F^- + CH_3F \rightarrow FCH_3 + F^-$, and $C_2H_5F \rightarrow C_2H_4 + HF$. The resulting reaction paths are compared with the paths obtained with the non-mass-weighted algorithm.

2. Theory

The steepest descent path in mass-weighted Cartesian coordinates (IRC) corresponds to the path obtained by stepping in the direction of the instantaneous acceleration. For other coordinate systems, the IRC can be obtained by transforming the steepest descent path in mass-weighted Cartesian coordinates. Entirely equivalently, the IRC can be constructed by following the instantaneous acceleration vector given by the equations of motion in that coordinate system.

The potential energy surface near the reaction path can be expanded as a Taylor series in internal coordinates

$$E(\mathbf{q}) = E'(\mathbf{q}') + \mathbf{g}^t\Delta q + \frac{1}{2}\Delta\mathbf{q}^t\mathbf{H}_q\Delta\mathbf{q} + \dots \quad (1)$$

where $\Delta\mathbf{q} = \mathbf{q} - \mathbf{q}'$, $\mathbf{H}_q$ is the Hessian matrix in internal coordinates and $\mathbf{g}$ is the gradient vector.

† Camile and Henry Dreyfus Scholar.

The classical kinetic energy in internal coordinates can be written as

$$2T = \Delta\dot{\mathbf{q}}^t\mathbf{G}^{-1}\Delta\dot{\mathbf{q}} \quad (2)$$

where T is the kinetic energy, $\mathbf{G}^{-1}$ is the inverse of the Wilson G matrix,[3] and $\Delta\dot{\mathbf{q}} = d\mathbf{q}/dt$ is the velocity vector in internal coordinates. Some complications in calculating the G matrix arise when the internal coordinates are specified using dummy atoms (see Appendix). The motion of this system can be determined from the Lagrangian equation:

$$\frac{d}{dt}\frac{\delta T}{\delta\Delta\dot{\mathbf{q}}} + \frac{\delta E(\mathbf{q})}{\delta\Delta\mathbf{q}} = 0 \quad (3)$$

Insertion of eqs 1 and 2 into (3) and truncating to second order yields

$$\mathbf{G}^{-1}\Delta\ddot{\mathbf{q}} + \mathbf{g} + \mathbf{H}_q\Delta\mathbf{q} = 0 \quad (4)$$

where $\Delta\ddot{\mathbf{q}} = d\Delta\dot{\mathbf{q}}/dt$ is the acceleration vector. Multiplying the left-hand side of eq 4 by G and rearranging gives the following expression for the acceleration vector:

$$\Delta\ddot{\mathbf{q}} = -(\mathbf{G}\mathbf{g} + \mathbf{G}\mathbf{H}_q\Delta\mathbf{q}) \quad (5)$$

For $\mathbf{q} = \mathbf{q}'$, a point on the reaction path, the acceleration vector and hence the displacement along the reaction path can be written as

$$\Delta\ddot{\mathbf{q}} = -\mathbf{G}\mathbf{g} \quad (6)$$

The reaction path can then be expressed as

$$\frac{d\mathbf{q}(s)}{ds} = -NGg \quad (7)$$

where N is a suitable normalization factor (see below). This gradient equation is the internal coordinate equivalent of the IRC of Fukui. The same expression has been obtained by Quapp and Heidrich[4] by applying a coordinate transformation to the steepest descent path in mass-weighted Cartesians.

(1) Fukui, K. *Acc. Chem. Res.* **1981**, *14*, 363.
(2) Gonzalez, C.; Schlegel, H. B. *J. Chem. Phys.* **1989**, *90*, 2154.
(3) Wilson, E. B.; Decius, G. C.; Cross, P. C. *Molecular Vibration*; McGraw-Hill: London, 1955.
(4) Quapp, W.; Heidrich, Dietmar. *Theor. Chim. Acta* **1984**, *66*, 245. Sana, M.; Reckinger, G.; Leroy, G. *Theor. Chim. Acta* **1981**, *58*, 145.

0022-3654/90/2094-5523$02.50/0

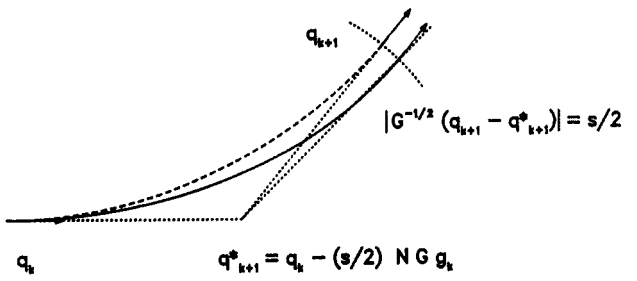

Figure 1. Reaction path following algorithm (solid line, true path; dashed line, approximate path; vectors point in the direction of the instantaneous acceleration, $-\mathbf{Gg}$). For an expression for the normalization factor N, see text.

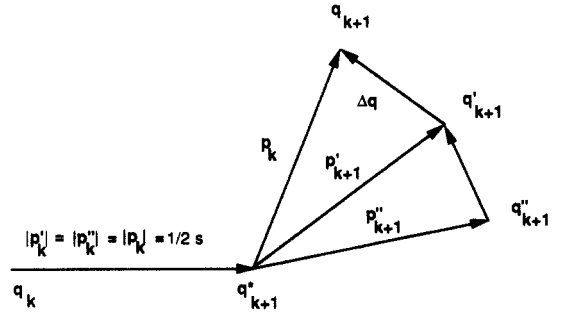

Figure 2. Definition of various vectors used in the reaction path following algorithm.

Figure 1 shows the basic features of the present reaction path following algorithm.[2] Starting with a point $\mathbf{q}_k$ of gradient $\mathbf{g}_k$ lying on the path, a new point $\mathbf{q}_{k+1}$ with gradient $\mathbf{g}_{k+1}$ is chosen so that the reaction path between $\mathbf{q}_k$ and $\mathbf{q}_{k+1}$ is an arc of a circle with the instantaneous accelerations $-\mathbf{Gg}_k$ and $\mathbf{Gg}_{k+1}$ tangent to the path. The pivot point, $\mathbf{q}^*_{k+1}$, is chosen by taking a step of length $(1/2)s$ along the vector $-\mathbf{Gg}_k$.

$$\mathbf{q}^*_{k+1} = \mathbf{q}_k - (1/2)sN\mathbf{Gg}_k \tag{8}$$

A new point on the path, $\mathbf{q}_{k+1}$, is obtained by a constrained minimization on the surface of the hypersphere centered at $\mathbf{q}^*_{k+1}$ and with radius $(1/2)s$. This constraint makes the residual gradient $\mathbf{Gg}_{k+1}$ parallel to $\mathbf{q}_{k+1} - \mathbf{q}^*_{k+1}$. The points $\mathbf{q}_k$, $\mathbf{q}^*_{k+1}$, and $\mathbf{q}_{k+1}$ form an isosceles triangle by construction; hence, the path between $\mathbf{q}_k$ and $\mathbf{q}_{k+1}$ is an arc of a circle. Even though the pivot point $\mathbf{q}^*_{k+1}$ is used in the constrained minimization, no gradient or energy calculation is performed at this point. As shown previously,[2] in the limit of small step sizes, this algorithm reproduces the correct tangent and curvature vectors, contrary to the reaction path following schemes of Ishida, Morokuma, and Komornicki,[5,6] and Müller and Brown.[7]

The lengths $\mathbf{q}_k$ to $\mathbf{q}^*_{k+1}$ and $\mathbf{q}^*_{k+1}$ to $\mathbf{q}_{k+1}$ (both which equal $(1/2)s$) can be computed in internal coordinates either with or without mass-weighting. While the latter is simpler, the former is more appropriate for the length of the intrinsic reaction path. By transformation of the length in mass-weighted Cartesian coordinates, it can be shown readily that the length in mass-weighted internal coordinates is $(\Delta\mathbf{q}^t\mathbf{G}^{-1}\Delta\mathbf{q})^{1/2}$. Hence, the normalization factor in eq 7 and 8 is

$$N = (g_k{}^tGg_k)^{-1/2} \tag{9}$$

Likewise the constraint on $\mathbf{q}_{k+1}$ is

$$[(\mathbf{q}_{k+1} - \mathbf{q}^*_{k+1})^t\mathbf{G}^{-1}(\mathbf{q}_{k+1} - \mathbf{q}^*_{k+1})]^{1/2} = (1/2)s \tag{10}$$

and the reaction path between $\mathbf{q}_k$ and $\mathbf{q}_{k+1}$ is an arc of a circle in mass-weighted internal coordinates. The length of the reaction path along the arc of the circle can be obtained by simple trigonometry. If θ is the angle between $\mathbf{q}^*_{k+1} - \mathbf{q}_k$ and $\mathbf{q}_{k+1} - \mathbf{q}^*_{k+1}$, then the arc length is $s\theta$ cot (θ).

Using a quadratic expansion of the energy surface in the vicinity of a point $\mathbf{q}'_{k+1}$, the instantaneous accleration $-\mathbf{Gg}_{k+1}$ at $\mathbf{q}_{k+1}$ can be written as

$$\mathbf{Gg}_{k+1} = \mathbf{Gg}'_{k+1} + \mathbf{GH}_q(\mathbf{q}_{k+1} - \mathbf{q}'_{k+1}) \tag{11}$$

where G is computed at $\mathbf{q}'_{k+1}$.[8] For the constrained optimization of $\mathbf{q}_{k+1}$, a number of vectors need to be defined (see Figure 2):

$$\mathbf{p}' = \mathbf{q}'_{k+1} - \mathbf{q}^*_{k+1} \tag{12}$$

$$\Delta\mathbf{q} = \mathbf{q}_{k+1} - \mathbf{q}'_{k+1} \tag{13}$$

$$\mathbf{p} = \mathbf{p}' + \Delta\mathbf{q} = \mathbf{q}_{k+1} - \mathbf{q}^*_{k+1} \tag{14}$$

At convergence, $\mathbf{Gg}_{k+1}$ must be parallel to $\mathbf{p}' + \Delta\mathbf{q}$. Thus, one can write

$$\mathbf{Gg}' + \mathbf{GH}_q\Delta\mathbf{q} - \lambda(\mathbf{p}' + \Delta\mathbf{q}) = 0 \tag{15}$$

where λ is the Lagrangian multiplier. In eq 15 as in the rest of the paper, where there is no ambiguity, the subscripts for the iteration counter k are omitted for simplicity. In eq 15 the dispalcement $\Delta\mathbf{q}$ must satisfy the following constraint:

$$(\mathbf{p}' + \Delta\mathbf{q})^t\mathbf{G}^{-1}(\mathbf{p}' + \Delta\mathbf{q}) = (\tfrac{1}{2}s)^2 \tag{16}$$

Multiplying the left-hand side of eq 15 by $\mathbf{G}^{-1/2}$ gives

$$\mathbf{G}^{1/2}\mathbf{g}' + \mathbf{G}^{1/2}\mathbf{H}_q\mathbf{G}^{1/2}\mathbf{G}^{-1/2}\Delta\mathbf{q} - \lambda(\mathbf{G}^{-1/2}\mathbf{p}' + \mathbf{G}^{-1/2}\Delta\mathbf{q}) = 0 \tag{17}$$

The terms $\mathbf{G}^{-1/2}\mathbf{p}'$, $\mathbf{G}^{1/2}\mathbf{g}'$, and $\mathbf{G}^{1/2}\mathbf{H}_q\mathbf{G}^{1/2}$ are displacements, gradients, and Hessian in mass-weighted internal coordinates. With the notation

$$\Delta\mathbf{q}_M = \mathbf{G}^{-1/2}\Delta\mathbf{q} \tag{18}$$

$$\mathbf{g}_M = \mathbf{G}^{1/2}\mathbf{g}' \tag{19}$$

$$\mathbf{H}_M = \mathbf{G}^{1/2}\mathbf{H}_q\mathbf{G}^{1/2} \tag{20}$$

$$\mathbf{p}_M = \mathbf{G}^{-1/2}\mathbf{p}' \tag{21}$$

eq 16 and 17 can be rewritten as

$$(\mathbf{p}_M + \Delta\mathbf{q}_M)^t(\mathbf{p}_M + \Delta\mathbf{q}_M) = (1/2s)^2 \tag{22}$$

$$(\mathbf{g}_M - \lambda\mathbf{p}_M) + (\mathbf{H}_M - \lambda\mathbf{I})\Delta\mathbf{q}_M = 0 \tag{23}$$

where I is the identity matrix. Solving eq 23 for $\Delta\mathbf{q}_M$ gives

$$\Delta\mathbf{q}_M = -(\mathbf{H}_M - \lambda\mathbf{I})^{-1}(\mathbf{g}_M - \lambda\mathbf{p}_M) \tag{24}$$

(8) The dependence of G on the coordinates is relatively small and has been neglected. Since convergence of constrained optimization is based on $\mathbf{G}\,\mathbf{g}'_{k+1}$, this assumption does not affect the final result.

(5) Ishida, K.; Morokuma, K.; Kormornicki, A. *J. Chem. Phys.* **1977**, *66*, 2153.
(6) Schmidt, M. W.; Gordon, M. S.; Dupuis, M. *J. Am. Chem. Soc.* **1985**, *107*, 2585.
(7) Müller, K.; Brown, L. D. *Theor. Chim. Acta* **1979**, *53*, 75.
(9) Broyden, C. G. *J. Inst. Math. Appl.* **1970**, *6*, 76. Fletcher, R. *Comput. J.* **1970**, *13*, 317. Goldfarb, D. *Math. Comput.* **1970**, *24*, 23. Shanno, D. F. *Math. Comput.* **1970**, *24*, 647.
(10) Davidon, W. *Math. Prog.* **1975**, *9*, 1. Fletcher, R.; Powell, M. J. D.; *Comput. J.* **1963**, *6*, 163.
(11) Scales, L. E. *Introduction to Non-linear Optimization*, MacMillan: Basingstoke, U.K. 1985.
(12) Fletcher, R. *Practical Methods of Optimization*; Wiley-Interscience: New York, 1980; Vol. 1.
(13) Frisch, M. J.; Head-Gordon, M.; Schlegel, H. B.; Raghavachari, K.; Binkley, J. S.; Gonzalez, C.; DeFrees, D.; Fox, D. J.; Whiteside, R. A.; Seeger, R.; Melius, C. F.; Kahn, L. R.; Stewart, J. J. P.; Fluder, E. M.; Topiol, S.; Pople, J. A. GAUSSIAN 88; Gaussian, Inc.: Pittsburgh, PA, 1988.
(14) Garrett, B. C.; Redmon, M. J.; Steckler, R.; Truhlar, D. G.; Baldridge, K. K.; Bartol, D.; Schmidt, M. W.; Gordon, M. S. *J. Phys. Chem.* **1988**, *92*, 1476.
(15) Yamashita, K.; Yamabe, T. *Int. J. Quant. Chem.* **1983**, *17*, 177.

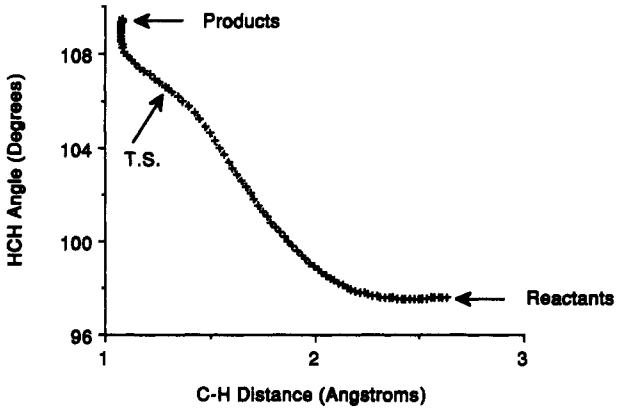

Figure 3. Reaction path for $CH_3 + H_2 \rightarrow CH_4 + H$ using a step size of 0.05 amu$^{1/2}$ bohr (+, mass-weighted internal coordinates; dots, mass-weighted Cartesian coordinates).

Notice that an expression identical with (23) is obtained if the variables $\Delta\mathbf{q}_M$, $\mathbf{p}_M$, $\mathbf{g}_M$, and $\mathbf{H}_M$ are substituted for $\Delta\mathbf{q}$, $\mathbf{p}'$, $\mathbf{g}$, and $\mathbf{H}$ in eq 10 of ref 2.

In order to find λ, eq 23 is introduced into the constraint (16), yielding

$$[\mathbf{p}_M - (\mathbf{H}_M - \lambda\mathbf{I})^{-1}(\mathbf{g}_M - \lambda\mathbf{p}_M)]^t \cdot [\mathbf{p}_M - (\mathbf{H}_M - \lambda\mathbf{I})^{-1}(\mathbf{g}_M - \lambda\mathbf{p}_M)] = (1/2s)^2 \quad (25)$$

Equation 25 can be solved iteratively to find the appropriate value of λ that satisfies the constraints. Working in the eigenvector space of $\mathbf{H}_M$, eq 25 reduces to

$$f(\lambda) = \sum_{j=1}^{n}\left[\frac{b_j\bar{p}_j - \bar{g}_j}{b_j - \lambda}\right]^2 - \left(\frac{1}{2}s\right)^2 = 0 \quad (26)$$

where $\bar{p}_j = \mathbf{p}_M^t \cdot \mathbf{V}_j$ and $\bar{g}_j = \mathbf{g}_M^t \cdot \mathbf{V}_j$ are the projections of $\mathbf{p}_M$ and $\mathbf{g}_M$ into the eigenvectors $\mathbf{V}_j$ of $\mathbf{H}_M$, b_j is the corresponding eigenvalue, and s is the step size. Equation 26 has multiple roots in λ; depending on the choice of root, the path can be followed uphill or downhill. A corresponding equation arises in methods developed by Cerjan and Miller,[16] Simons et al.,[17] and Baker[18] for finding transition states/minima by following valleys uphill/downhill. For the present application of following the reaction path downhill from the transition state, λ must be less than the lowest eigenvalue of the Hessian. The optimum value of λ is found by a bracketing search followed by a binary search;[19] then $\Delta\mathbf{q}_M$ is calculated by means of eq 24, and a new point on the path $\mathbf{q}_{k+1}$ is determined by

$$\mathbf{q}_{k+1} = \Delta\mathbf{q} + \mathbf{q}'_{k+1} = \mathbf{G}^{1/2}\Delta\mathbf{q}_M + \mathbf{q}'_{k+1} \quad (27)$$

The optimization procedure given by eq 11–27 is continued until $\Delta\mathbf{q}_M$ and the component of the gradient tangent to the hypersphere, $\mathbf{g}_M - \mathbf{p}^t\mathbf{g}_M/|\mathbf{p}|^2$, becomes smaller than a preestablished cutoff. As discussed previously,[2] the use of a linear search before each quasi-Newton step results in a marked improvement of the stability and efficiency of the optimization. The linear search consists of a polynomial interpolation between the current point and the previous point along the surface of the sphere of radius $^1/_2s$ centered at q^*_{k+1}.

The Hessian $\mathbf{H}_q$ is calculated analytically only at the transition state. At all other point, it is updated by the BFGS formula[9]

$$\mathbf{H}'_q = \mathbf{H}''_q + \frac{\Delta\mathbf{g}'\cdot\Delta\mathbf{g}'^t}{\Delta\mathbf{g}'^t\Delta_q'} - \frac{(\mathbf{H}''_q\Delta\mathbf{q}')\cdot(\Delta\mathbf{q}'^t\mathbf{H}''_q)}{\Delta\mathbf{q}'^t\mathbf{H}''_q\Delta\mathbf{q}'} \quad (28)$$

(16) Cerjan, C. J.; Miller, W. H. *J. Chem. Phys.* **1981**, *75*, 2800.
(17) Simons, J.; Jørgensen, P.; Taylor, H.; Ozment, J. *J. Phys. Chem.* **1983**, *87*, 2745. Banerjee, A.; Adams, N.; Simons, J. *J. Phys. Chem.* **1985**, *89*, 52.
(18) Baker, J. *J. Comput. Chem.* **1986**, *7*, 385.
(19) The accuracy in the determination of λ must be such that the constraint is satisfied more accurately than the stopping criteria for the minimization.

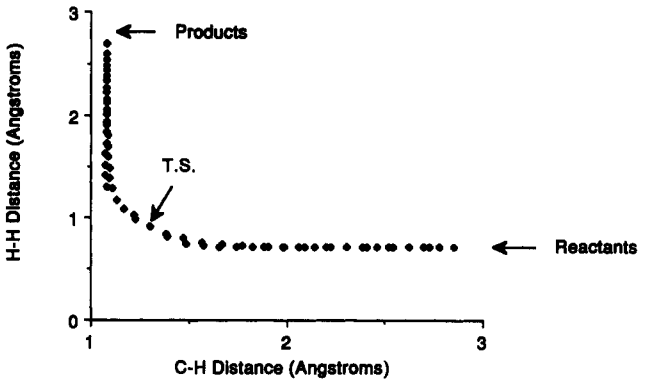

Figure 4. Reaction path for $CH_3 + H_2 \rightarrow CH_4 + H$ using a step size of 0.2 amu$^{1/2}$ bohr: H–H distance versus C–H distance (open diamonds, internal coordinates with mass-weighting; filled diamonds, internal coordinates without mass-weighting).

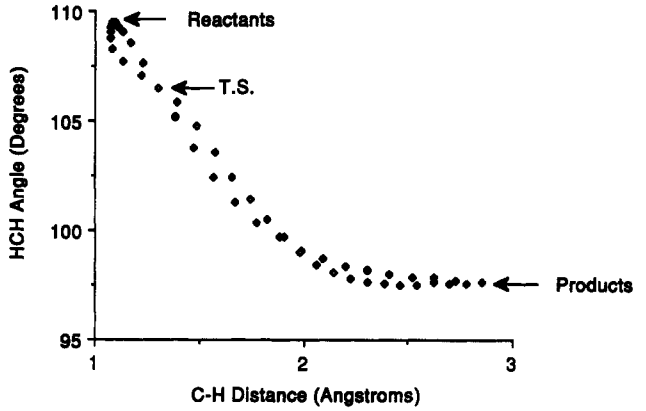

Figure 5. Reaction path for $CH_3 + H_2 \rightarrow CH_4 + H$ using a step size of 0.2 amu$^{1/2}$ bohr: HCH angle versus C–H distance (open diamonds, internal coordinates with mass-weighting; filled diamonds, internal coordinates without mass-weighting).

with $\Delta\mathbf{g}' = \mathbf{g}' - \mathbf{g}''$, and $\Delta\mathbf{q}' = \mathbf{q}' - \mathbf{q}''$. The primes and double primes refer to the current and previous points, respectively. Contrary to methods such as DFP,[10] this updating scheme produces Hessian changes that are positive definite,[11,12] which makes it suitable for minimizations.

3. Results

The present algorithm has been implemented and interfaced with the development version of GAUSSIAN 88 system of programs.[13] For four different reactions, reaction paths have been obtained in both mass-weighted and non-mass-weighted internal coordinates by using a step size of 0.2 amu$^{1/2}$ bohr. In each case, the algorithm is started at the transition state, where the analytical Hessian is used. In subsequent points, the Hessian is updated by the BFGS formula.[9] The HF/STO-3G optimized transition state for $CH_3 + H_2 \rightarrow CH_4 + H$ was taken from ref 14; all other transition-state structures are the same as in ref 2.

Figure 3 depicts variations of the HCH angle versus the C–H distance for the reaction $CH_3 + H_2 \rightarrow CH_4 + H$ obtained with mass-weighted internal coordinates (+ symbols) and with mass-weighted Cartesian coordinates using Euler steps (dots). Both paths were calculated with a step size of 0.05 amu$^{1/2}$ bohr at the HF/STO-3G level of theory. The fact that there is no difference between the paths and that these paths are the same as reported in the literature[14,15] indicates that the mass-weighted internal coordinates reaction path algorithm has been implemented properly. The correct behavior of the algorithm for the other reactions has also been verified by comparison with the mass-weighted Cartesian approach using Euler steps. Figure 4 is a plot of the H–H distance against the CH_3–H distance, while Figure 5 shows the relation between the HCH angle against the H–H distance. The difference between the mass-weighted internal coordinate reaction path (open diamonds) and the non-mass-weighted internal coordinate path (filled diamonds) is small for

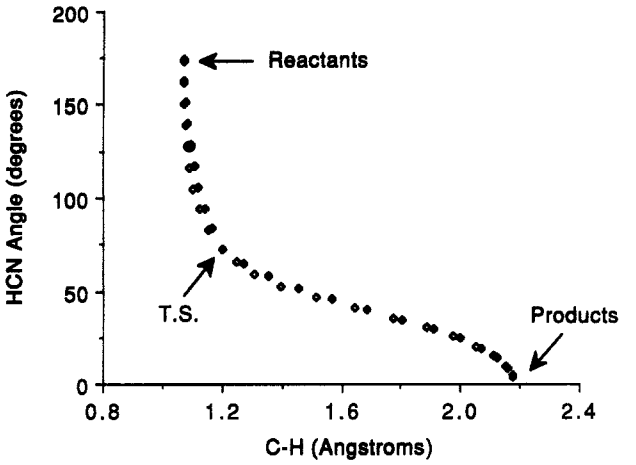

Figure 6. Reaction path for HCN → HNC using a step size of 0.2 amu$^{1/2}$ bohr: HCN angle versus C–H distance (open diamonds, internal coordinates with mass-weighting; filled diamonds, internal coordinates without mass-weighting).

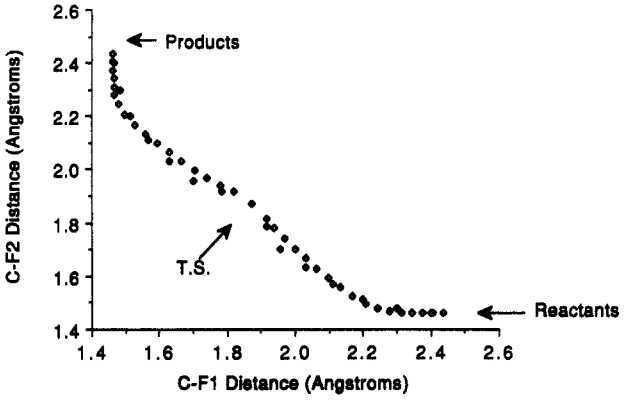

Figure 7. Reaction path for $F^- + CH_3F \rightarrow FCH_3 + F^-$ using a step size of 0.2 amu$^{1/2}$ bohr: $C-F_2$ distance versus $C-F_1$ distance (open diamonds, internal coordinates with mass-weighting; filled diamonds, internal coordinates without mass-weighting).

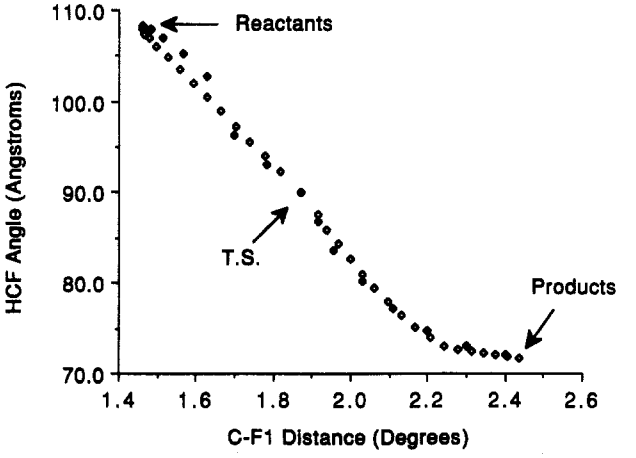

Figure 8. Reaction path for $F^- + CH_3F \rightarrow FCH_3 + F^-$ using a step size of 0.2 amu$^{1/2}$ bohr: HCF_1 angle versus $C-F_1$ distance (open diamonds, internal coordinates with mass-weighting; filled diamonds, internal coordinates without mass-weighting).

H–H versus CH_3–H but noticeable for ∠HCH versus CH_3–H.

Figure 6 shows a plot of HCN angle versus the HC distance in the HCN → HNC isomerism (HF/STO-3G). Figures 7 and 8 show the changes of the C–F distances and the HCF angle along the reaction path for the fluoride ion attack to methyl fluoride (HF/4-31G level). In all of these cases, reaction paths with and without mass-weighting do not seem to differ very much. By contrast, the four-centered elimination process $CH_3CH_2F \rightarrow CH_2CH_2F + HF$, Figures 9–11, shows large differences between

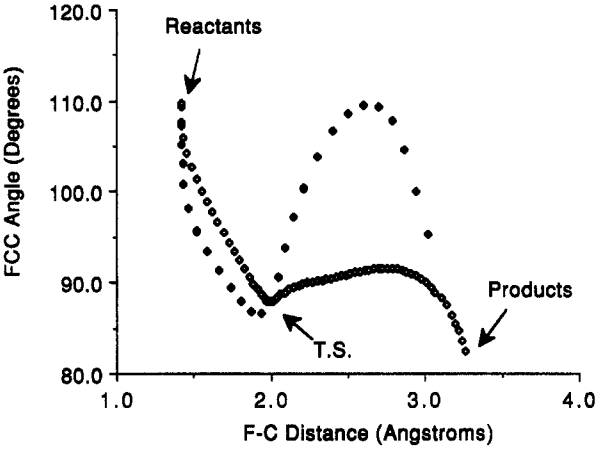

Figure 9. Reaction path for $CH_3CH_2F \rightarrow CH_2CH_2 + HF$ using a step size of 0.2 amu$^{1/2}$ bohr: FCC angle versus C–F distance (open diamonds, internal coordinates with mass-weighting; filled diamonds, internal coordinates without mass-weighting).

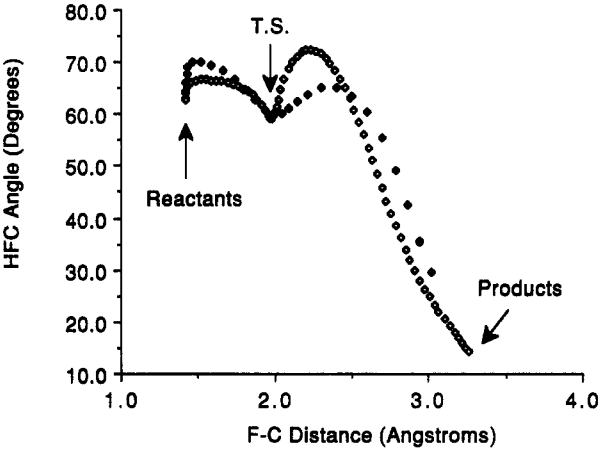

Figure 10. Reaction path for $CH_3CH_2F \rightarrow CH_2CH_2 + HF$ using a step size of 0.2 amu$^{1/2}$ bohr: HFC angle versus C–F distance (open diamonds, internal coordinates with mass-weighting; filled diamonds, internal coordinates without mass-weighting).

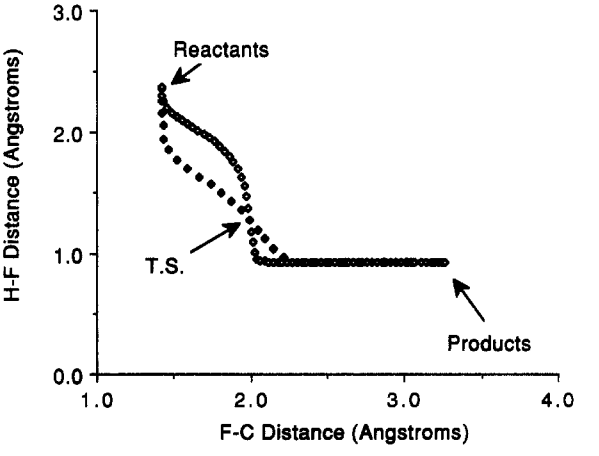

Figure 11. Reaction path for $CH_3CH_2F \rightarrow CH_2CH_2 + HF$ using a step size of 0.2 amu$^{1/2}$ bohr: HF distance versus C–F distance (open diamonds, internal coordinates with mass-weighting; filled diamonds, internal coordinates without mass-weighting).

the mass-weighted (open diamonds) and non-mass-weighted (filled diamonds) paths. This is because both light and heavy atoms undergo large displacements in the course of the reaction. Mass-weighting reduces the motion of the carbon and fluorine atoms and enhances the motion of the hydrogens. Thus changes in the F–C distance and FCC angle are smaller and changes in the H–F distance are larger as the reaction proceeds along the path.

Acknowledgment. This work was supported by a grant from the National Science Foundation (CHE-87-11901) and by the Pittsburgh Supercomputer Center.

Appendix

The use of dummy atoms in defining internal coordinates gives rise to some complications in converting mass-weighted Cartesian coordinates to internals. For a nonlinear molecule with n_A real atoms and n_D dummy atoms, there are only $3n_A - 6$ internal coordinates that may be varied independently and $3n_D$ internal coordinates that must be fixed. Symmetry may require additional coordinates to be fixed. The conversion between Cartesian and internal coordinates is written in terms of Wilson's **B** matrix,

$$\Delta \mathbf{q} = \mathbf{B}\Delta \mathbf{x} \tag{A1}$$

The **B** matrix can be partitioned into blocks dealing with the displacement of the real atoms, $\Delta \mathbf{x}_A$, and the dummy atoms, $\Delta \mathbf{x}_D$; let **P** be the projector for the internal coordinates that are independently variable, $\mathbf{Q} = \mathbf{I} - \mathbf{P}$ the projector for the internal coordinates that must remain constant, and **I** the identity matrix; then

$$\Delta \mathbf{q} = \mathbf{P}(\mathbf{B}_A \Delta \mathbf{x}_A + \mathbf{B}_D \Delta \mathbf{x}_D) \tag{A2}$$

$$\mathbf{Q}(\mathbf{B}_A \Delta \mathbf{x}_A + \mathbf{B}_D \Delta \mathbf{x}_D) = 0 \tag{A3}$$

The displacement of the real atoms depend on the displacements of the variable internal coordinates. The displacements of the dummy atoms must be such that the remaining internal coordinates are constant. Since the number of fixed coordinates is greater than or equal to $3n_D$, eq A3 must be solved for $\Delta \mathbf{x}_D$ in a least-squares manner:

$$\Delta \mathbf{x}_D = -(\mathbf{B}_D^t \mathbf{Q} \mathbf{B}_D)^{-1} \mathbf{B}_D^t \mathbf{Q} \mathbf{B}_A \Delta \mathbf{x}_A \tag{A4}$$

Substitution into eq A2 yields

$$\Delta \mathbf{q}_v = \mathbf{B}' \Delta \mathbf{x}_A, \quad \mathbf{B}' = \mathbf{P}\mathbf{B}_A - \mathbf{P}\mathbf{B}_D(\mathbf{B}_D^t \mathbf{Q} \mathbf{B}_D)^{-1} \mathbf{B}_D^t \mathbf{Q} \mathbf{B}_A \tag{A5}$$

This modified **B** matrix, **B'**, can be used to compute the **G** matrix, $\mathbf{G}' = \mathbf{B}' m^{-1} \mathbf{B}'^t$, since the masses of the dummy atoms are no longer involved.

Thermal Decomposition Processes for Silanol

Mark S. Gordon* and Lisa A. Pederson

Department of Chemistry, North Dakota State University, Fargo, North Dakota 58105
(Received: November 1, 1989; In Final Form: March 2, 1990)

Six alternative decomposition modes of silanol are examined with ab initio electronic structure theory. Geometries determined at the MP2/6-31G(d,p) level of computation and single-point energetics obtained with MP4/MC-311G(d,p) wave functions predict that the 1,1- and 1,2-eliminations of molecular hydrogen are both thermodynamically and kinetically competitive, with all other processes requiring at least 10 kcal/mol more energy to occur. At the highest level of theory, silanone is predicted to be 2.7 kcal/mol lower in energy than hydroxysilylene.

I. Introduction

The molecule silanol, SiH_3OH, is the simplest saturated species containing an SiO bond. It is, in addition, the simplest prototype for silicic acid, $Si(OH)_4$, the starting molecule for siloxane polymerization processes to form $(Si-O)_n$ polymers. Silanol is also a candidate for an alternative to silane as a precursor to chemical vapor deposition.[1] It is of considerable interest to develop an understanding of the mechanisms and energetics of the processes summarized above. Previous papers from this[2] and other[3] laboratories have considered potential intermediate steps in the silanol and silicic acid polymerization process. A key step in gaining a full understanding of Si–O reactivity and the nature of the Si–O bond is to analyze the alternative thermal decomposition processes of the parent silanol.

The thermal decompositions of a number of related compounds have already been investigated with theoretical techniques. These include silane,[4] ethane,[5] methylsilane,[6] disilane,[7] silylamine,[8] methyl and ethyl mercaptan,[9] ethylsilane,[10] and chloromethylsilane.[11] When one of the atoms in the parent molecule is a saturated Si, it is generally found that 1,2-elimination of molecular hydrogen to form a silene has a much higher barrier than the 1,1-H_2 elimination from the silicon to form a silylene, even in those cases for which the 1,2-process may lead to thermodynamically favored products. It has also been found that the two hydrogens in the 1,2-elimination process prefer to leave in an asymmetric manner. Viewed in the reverse direction as an addition of H_2 across a double bond, the H_2 tends to attack in such a manner that both H's are closer to the less electronegative partner in the double bond.

In the present work, the following alternative decomposition processes of silanol are considered:

$$SiH_3OH \rightarrow SiH_3O + H \tag{1}$$

$$\rightarrow SiH_2OH + H \tag{2}$$

$$\rightarrow SiH_3 + OH \tag{3}$$

$$\rightarrow H_2SiO + H_2 \tag{4}$$

$$\rightarrow HSiOH + H_2 \tag{5}$$

$$\rightarrow SiH_2 + H_2O \tag{6}$$

The first three of these reactions are homolytical cleavages of a

(1) (a) Coltrin, M. E.; Kee, R. J.; Miller, J. A. *J. Electrochem. Soc.* **1984**, *131*, 425. (b) Steinwandel, J.; Hoeschele, J. *Chem. Phys. Lett.* **1985**, *116*, 25.
(2) (a) Gordon, M. S.; Davis, L. P.; Burggraf, L. W.; Damrauer, R. *J. Am. Chem. Soc.* **1986**, *108*, 7889. (b) Davis, L. P.; Burggraf, L. W.; Gordon, M. S. *J. Am. Chem. Soc.* **1988**, *110*, 3056. (c) Damrauer, R.; Davis, L. P.; Burggraf, L. W.; Gordon, M. S. *J. Am. Chem. Soc.* **1988**, *110*, 6601.
(3) (a) Burggraf, L. W.; Davis, L. P. *Chemically Modified Surfaces*; Gordon and Breach Science: New York, 1986; pp 157-187. (b) Davis, L. P.; Burggraf, L. W. *Science of Ceramic Chemical Processing*; Wiley: New York, 1986; pp 400-411. (c) Burggraf, L. W.; Davis, L. P. *Mater. Res. Soc. Symp. Proc.* **1986**, *73*, 529. (d) Davis, L. P.; Burggraf, L. W. *Ultrastructure Processing of Advanced Ceramics*; Wiley: New York, 1988; pp 367-368.
(4) Gordon, M. S.; Gano, D. R.; Binkley, J. S.; Frisch, M. J. *J. Am. Chem. Soc.* **1986**, *108*, 2191.
(5) Truong, T. N.; Gordon, M. S.; Pople, J. A. *Chem. Phys. Lett.* **1986**, *130*, 245.
(6) Gordon, M. S.; Truong, T. N. *Chem. Phys. Lett.* **1987**, *142*, 110.
(7) Gordon, M. S.; Truong, T. N.; Bonderson, E. K. *J. Am. Chem. Soc.* **1986**, *108*, 1421.
(8) Truong, T. N.; Gordon, M. S. *J. Am. Chem. Soc.* **1986**, *108*, 1775.
(9) Baldridge, K. K.; Gordon, M. S.; Johnson, D. E. *J. Phys. Chem.* **1987**, *91*, 4145.
(10) Francisco, J. S.; Schlegel, H. B. *J. Chem. Phys.* **1988**, *88*, 3736.
(11) Nagase, S.; Kudo, T. *J. Chem. Soc., Chem. Commun.* **1983**, *6*, 363.

0022-3654/90/2094-5527$02.50/0